PAPER

Evolution of electronic and magnetic properties of nominal magnetite nanoparticles at high pressure probed by x-ray absorption and emission techniques

IOP Publishing Journal of Physics: Condensed Matter
J. Phys.: Condens. Matter **31** (2019) 255301 (12pp) https://doi.org/10.1088/1361-648X/ab111d

Evolution of electronic and magnetic properties of nominal magnetite nanoparticles at high pressure probed by x-ray absorption and emission techniques

Kalpani Werellapatha[1,7], Carlos A Escanhoela Jr[2,3], Gilberto Fabbris[2], Daniel Haskel[2], Alexei Ankudinov[4] and Paul Chow[5,6]

[1] Department of Physics and Astronomy, University of Maine, Orono, ME 04469, United States of America
[2] Advanced Photon Source, Argonne National Laboratory, Argonne, IL 60439, United States of America
[3] Brazilian Synchrotron Light Laboratory (LNLS), Campinas, SP 13083-970, Brazil
[4] Department of Physics, Box 351560, University of Washington, Seattle, WA 98195, United States of America
[5] Geophysical Laboratory, Carnegie Institution of Washington, 5251 Broad Branch Road NW, Washington, DC 20015, United States of America
[6] HPCAT, Carnegie Institution of Washington, Building 434E, 9700 South Cass Avenue, Argonne, IL 60439, United States of America

E-mail: kwerella@alumni.nd.edu

Received 19 October 2018, revised 2 March 2019
Accepted for publication 19 March 2019
Published 8 April 2019

Abstract

We present a study of electronic and magnetic properties of nominal magnetite nanoparticles (NPs) (~6 nm) at high pressure in the presence of silicon pressure medium using x-ray absorption near edge structure (XANES), x-ray magnetic circular dichroism (XMCD) and non-resonant x-ray emission spectroscopy (XES). XANES data show a reduction of Fe charge state, a change in local environment around Fe at tetrahedral sites, and a reduced occupation of Fe 4*p* orbitals, not seen in previous pressure studies of bulk magnetite. XMCD data show a continuous magnetic moment reduction of ~50% between ambient pressure and 20 GPa, similar to what was observed in previous bulk magnetite studies. XES spectra of NPs indicate a gradual change in spin configuration away from the high-spin state consistent with a postulated charge transfer from Fe 4*p* to 3*d* states and the observed reduction in XMCD signal. Taken together, the results point to substantial differences in the response of electronic and magnetic properties of the nano-counterparts of bulk magnetite at high pressure.

Keywords: x-ray absorption spectroscopy, x-ray magnetic circular dichroism, x-ray emission spectroscopy, magnetite nanoparticles, high pressure physics, diamond anvil cells

(Some figures may appear in colour only in the online journal)

1. Introduction

Nanoparticles (NPs) are ultrafine particles with dimensions ranging from 1 nm to 100 nm [1]. Due to their small size, a large fraction of atoms will be near the surface resulting in significant differences in atomic, electronic, magnetic, physical and chemical reactivity compared to their bulk counterparts [2]. These properties of NPs are further modified when exposed to extreme conditions such as high pressure and temperature environments [3].

Iron-oxide magnetite (Fe_3O_4) is a naturally occurring, iron-rich, magnetic mineral. Nano counterparts of magnetite

[7] Author to whom any correspondence should be addressed.

exist in a thermodynamically stable phase in the environment and are ubiquitous [4]. Response of electronic, magnetic and structural properties of such minerals to extreme conditions is important in geology, to understand mineral properties at conditions found deep inside the earth. Additionally, tailoring the strong electron interactions present in these materials with pressure can lead to metal-insulator, high-spin to low-spin, and superconducting transitions not attainable at ambient conditions (pressure drives these transitions by tuning electronic bandwidth and crystal electric fields). Of particular interest is how these transitions may be affected by finite size and surface effects present in NPs [5].

Although many investigations into electronic and magnetic properties of bulk magnetite at high pressure have been conducted [6–11], little is known regarding their nano-counterparts. A recent study that used x-ray magnetic circular dichroism (XMCD), x-ray diffraction (XRD) and x-ray emission spectroscopy (XES) on bulk magnetite powder showed a pressure-induced magnetic transition in the 12–16 GPa range, that was independent of temperature (40–300 K range) [6]. The rather abrupt change in XMCD signal in this pressure range was attributed to a high- to intermediate-spin transition. A follow-up XMCD study that reached 41 GPa at room temperature showed instead a more gradual transition taking place in the 10–15 GPa range and deemed inconsistent with a spin transition [7].

In the current study, we show that high pressure induces further modifications in electronic and magnetic properties of NPs, already induced by size. Therefore, this study is a first step towards the understanding of electronic and magnetic properties of nano-sized counterparts of bulk magnetite at high pressure. Our aim is to follow the footsteps of previous investigations on bulk magnetite at high pressure, identify and compare mechanisms that describe differences that occur in NPs compared to their bulk counterparts.

Bulk magnetite has a cubic inverse spinel structure with tetrahedral sites occupied by Fe^{3+} ions and octahedral sites occupied by equal number of Fe^{2+} and Fe^{3+} ions [12, 13]. Bulk Maghemite (γ-Fe_2O_3), similar in structure to bulk magnetite, has all the cations in the trivalent state [14]. XRD patterns of both bulk and nano structures of magnetite and maghemite are similar making it hard to distinguish between the two [15]. Iron oxide magnetic NPs are frequently characterized by combining infrared (IR) and Mössbauer spectroscopies with XRD and transmission electron microscopy (TEM) [16, 17]. As a result of nanoscale effects originating from very small crystallite sizes, large surface-to-volume ratio, near-surface relaxation and local lattice distortions, broadening and smearing out of Bragg reflections in the XRD patterns or in the Mössbauer lines are frequent [15]. Therefore, the standard methods used for bulk crystal structure determination may not be suitable for their nano-counterparts. Similarly, there have been disagreements regarding the capability of both Raman and IR spectroscopies to distinguish Fe_3O_4 from γ-Fe_2O_3 [18–21]. Therefore, more powerful techniques based on x-ray absorption and emission spectroscopy (XAS/XES), that are known for being extremely sensitive to oxidation state, local environment around the atom being probed, magnetic configuration, and elemental and chemical selectivity may promise more reliable results [15], especially at high pressure conditions.

We use Fe *K*-edge x-ray absorption near edge structure (XANES) and XMCD measurements to probe electronic and magnetic properties of magnetite NPs. To reach high pressure, the sample is placed in a diamond anvil cell (DAC). Despite its lower dichroic contrast, Fe *K*-edge measurements allow penetrating the diamond anvils, not possible at the Fe $L_{2,3}$ edges. Also, the XMCD spectra of both bulk magnetite and maghemite at the Fe $L_{2,3}$-edges show rather similar fine structure, in contrast to more distinguishable features at the Fe *K*-edge [15]. Although electric dipole transitions at the Fe *K*-edge do not directly couple the initial 1*s* core state to the magnetic 3*d* states of the resonant atom, changes in 3*d* moment affect the exchange splitting of the 4*p* band. Therefore, the *K*-edge XMCD signal can be used as a measure of the magnetic moment under pressure [7, 22–24].

In addition, to probe for spin transitions [6] in 3*d* orbitals of Fe, we use non-resonant XES. The spin state of Fe is measured via high resolution Fe K_β emission line. Being a very sensitive technique to the local moment, XES leverages the exchange interaction between the 3*p* core hole and the 3*d* local magnetic moment of Fe in the final state of the x-ray emission process. This exchange interaction splits the emission line into two peaks, one at 7058 eV and a small satellite peak ($K_{\beta'}$) ~12 eV below it. The intensity of the small satellite peak is proportional to the number of unpaired electrons in the 3*d* orbitals.

2. Experimental details

2.1. Material synthesis

Iron oxide NPs of average diameter 6 nm were prepared following Kim *et al* [25] under non-oxidizing environments. Ferric chloride hexahydrate ($FeCl_3{\cdot}6H_2O$, >99%) and Ferrous chloride tetrahydrate ($FeCl_2{\cdot}4H_2O$, > 99%) were used to prepare Fe^{3+} and Fe^{2+} solutions. A volume of 5 ml of solution containing 0.1 M Fe^{2+} and 0.2 M Fe^{3+} was added dropwise to 50 ml of NaOH under vigorous mechanical stirring for 30 min at room temperature conditions. The precipitated powders were collected by centrifugation and were washed with distilled water to remove the ligands (N_2 gas was used to remove oxygen dissolved in water prior to washing). The precipitated NPs were dried under non-oxidizing conditions. They were kept in PTFE tubes under non-oxidizing environments, sealed in the dark for up to one month to avoid any light-induced reactions. The dried powders were separated using a 20 μm sieve before placing them in the DAC for high pressure experiments.

2.2. Characterization

The NP sample was characterized using powder XRD with a PAN Analytical X-Pert Pro diffractometer that uses a monochromatic x-ray beam with a Cu K_α source. The XRD pattern of NPs on a glass plate was collected from 5° to 70° in 2θ. Due to the large background signal from the amorphous glass

material, only the XRD data above 20° is shown. Scherrer's equation was used to determine the average diameter of the NPs. Raman spectroscopy was used to extract phase information. Raman spectra were recorded on a Renishaw Raman Imaging Microscope System 1000. The system consists of a diode laser with $\lambda_{ex} = 785$ nm. All Raman spectra were recorded at room temperature. A ~10 s spectral acquisition time with a low laser power (~6 mW) was chosen to prevent heat induced phase transitions. Spectral range was chosen below 1000 cm^{-1}, to include only the important diagnostic phonon modes used to differentiate various iron oxides [18]. NPs were imaged with TEM using a 200 kV JEOL 2100 which uses a LaB_6 filament type. The sample was sonicated overnight and was dispersed in ethanol. It was prepared for imaging by placing one drop of dilute particle suspension on a carbon coated (300 mesh) TEM copper grid at room temperature. Magnetic properties of the NPs were determined using a Quantum Design SQUID magnetometer. Hysteresis loops ($M(H)$ curve) were measured under a maximum applied magnetic field of ±80 kOe at room temperature to obtain the saturation magnetization. Hysteresis loop was normalized to iron-oxide mass. Saturation magnetization (M_s) was obtained by extrapolating the $M(H)$ curve to zero field, from the high-field range where the magnetization changes linearly with applied field as, $M(H) \sim M_s + \chi_d H$, where χ_d is the high field differential susceptibility that accounts for the surface spin disorder [26].

XANES and XMCD measurements on iron-oxide NPs across the Fe *K*-absorption edge energy (7112 eV) were conducted in transmission mode at beamline 4-ID-D of the Advanced Photon Source, Argonne National Laboratory. A double crystal Si(1 1 1) monochromator was used, and higher energy harmonics were rejected by both detuning the second crystal by 5.35 arcsec as well as using toroidal Pd-coated and flat Si harmonic rejection mirrors at 3.1 mrad incidence angle. Photodiodes were used to measure incident (transmitted) photon flux before (after) the sample. An Fe foil was used as reference to check for any drifts in the monochromator energy, found to be smaller than 0.1 eV (the monochromator energy resolution is ~1 eV). An aperture was used to further reduce the focused beam size to approximately 30 × 30 μm^2. Further details of the beamline optics and instrumentation can be found in Haskel *et al* [27]. The DAC was configured with a partially perforated anvil opposite a mini-anvil placed atop a fully perforated anvil in order to reduced attenuation of the x-ray beam in the diamond anvils and maintain on-axis optical axis for pressure calibration using the Ruby fluorescence method (anvil partial perforations are opaque) [27]. Culet size of the diamond anvils was ~300 μm while the rhenium gasket hole size (sample chamber size) was ~140 μm. The particles were separated using a sieve with 20 μm opening before loading them in the DAC. The NPs were mixed with Ruby balls used as *in situ* pressure manometer, and silicone oil as pressure transmitting medium following Ding *et al* [6]. We measured XANES spectra in the absence of a magnetic field increasing the pressure of the sample from ~2 GPa to ~20 GPa at 1–2 GPa intervals at room temperature. Sample pressure was measured before and after data collection at each pressure point. After reaching the maximum pressure, the data were collected on pressure release at 1–2 GPa intervals to check for irreversible changes in the XANES spectra. Simultaneous XANES and XMCD measurements in the presence of a magnetic field of 4 T were done at pressures selected based on the XANES measurements obtained in the absence of a magnetic field.

The XES experiments were performed with silicone as pressure medium in a Mao-type DAC, at the 16-ID-D station of HPCAT sector 16, APS, Argonne National Laboratory. The incident monochromatic x-ray beam was set at 11.6 keV with a ~1 eV energy resolution. The Fe K_β emission spectra were collected using a Si(3 3 3) crystal analyzer and Si(Sn) x-ray detector in a backscattering geometry.

Theoretical XMCD simulations were performed with the FEFF8 code [28]. The self-consistency of the FEFF8 code is crucial for predictive Fermi level position and accounts for charge transfer between atoms. Spin density mainly comes from Fe 3*d* electrons with well localized orbitals. The total 3*d* spin projection on the x-ray propagation direction for each Fe atom in the structure is specified in the FEFF8 input file. The total spin density in FEFF8 is constructed as a superposition of individual atomic spin densities. The *K*-edge XMCD signal can be viewed as a probe of orbital moment in the unoccupied *p*-states of the absorbing atom. FeFF8 calculates individual XMCD contributions from each atom in the structure and can be used to separate contributions from inequivalent crystal sites.

The procedure for reduction of XANES spectra can be found in Bunker *et al* [29]. Once normalized to the edge jump, the pre-edge peaks were integrated using numerical integration techniques within a specified energy range and the shift in main-edge energy of NPs with pressure were determined with respect to the edge energy of bulk maghemite. XES spectra were background subtracted and were normalized to unity by the area of the spectrum. For integrated absolute difference method (IAD), a difference spectrum was obtained by subtracting a reference spectrum (spectrum at ambient conditions without silicon oil) from spectra at each pressure value. The integral of the absolute value of the difference spectrum was calculated as the IAD according to Vanko *et al* [30].

3. Results

3.1. NP characterization

XRD data of the NPs in figure 1(a) shows peaks corresponding to the spinel structure and a mean NP diameter of 7.1 ± 0.6 nm, calculated using Scherrer's equation. The lattice parameter has been calculated as 8.36 ± 0.02 Å. Raman spectroscopy can be used as an effective tool to fingerprint phases of magnetite and maghemite due to distinct features in the spectra [19]. Raman spectra of NPs in figure 1(b) exhibit broad phonon modes that correspond to those of bulk maghemite, around 365 cm^{-1}, 511 cm^{-1} and 700 cm^{-1} as listed in previous literature [18, 19, 31, 32]. This result is also confirmed by XANES data of NPs (figure 1(c)) compared with bulk standards of maghemite and magnetite. The TEM image in figure 1(d) suggests the particles were either rounded or rounded hexagonal. The sample was too thick to produce images with distinguishable lattice

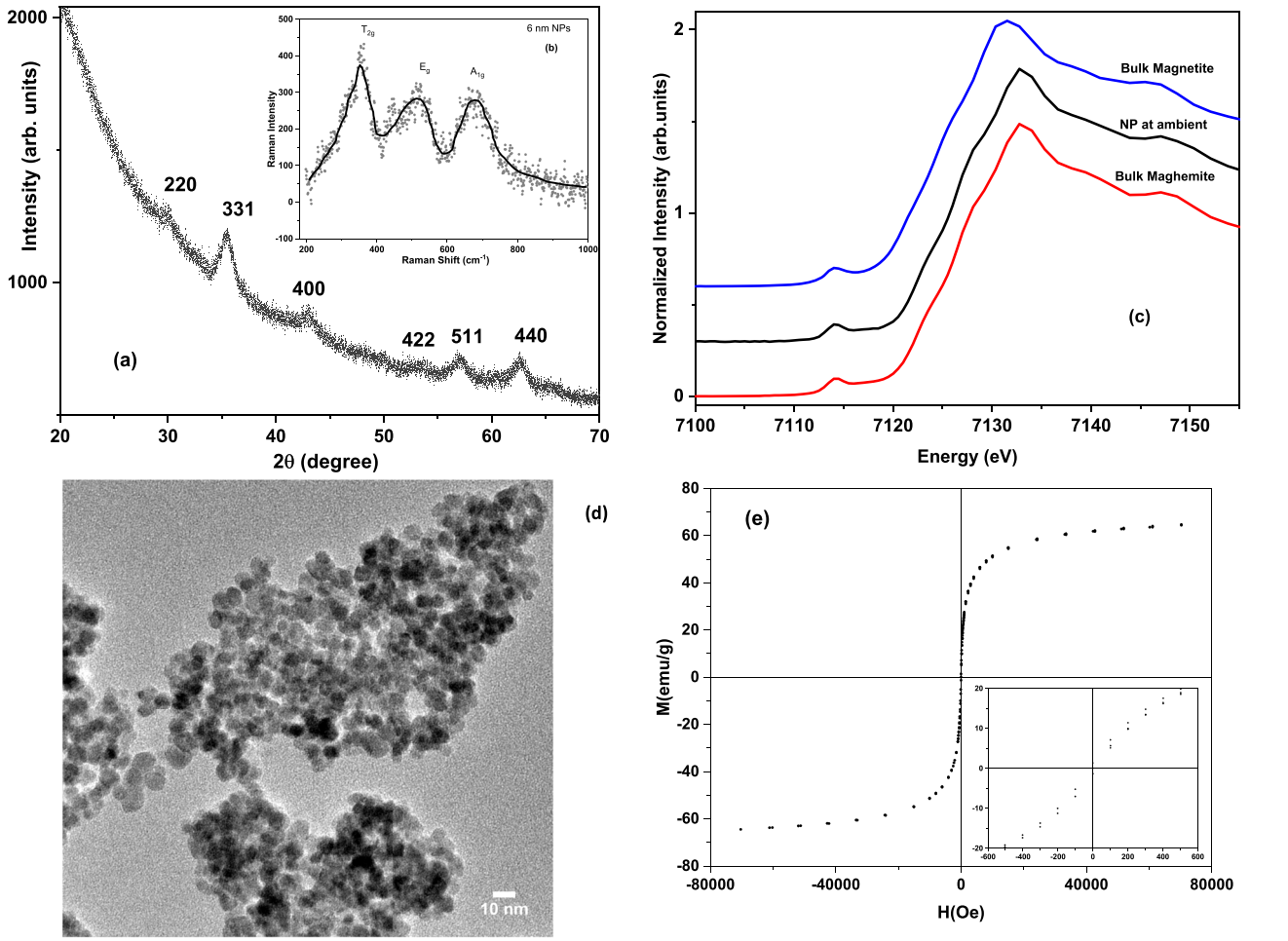

Figure 1. (a) XRD spectra of NPs (b) Raman spectra with phonon peak assignments at ambient conditions (c) XANES spectra of NPs at ambient conditions (called 'ambient') compared with bulk standards (d) TEM image of NPs (e) magnetization (M) versus applied magnetic field (H) for NPs.

fringes. The saturation magnetization calculated from the hysteresis loop of NPs (figure 1(e)) at room temperature is ~2.3 μ_B per formula unit.

3.2. Interaction of NPs with silicon oil

We checked for any interactions between NPs and silicone oil using Raman and XES spectroscopy. Assuming spherical shape of NPs, we estimated the surface to core volume fraction to be about 0.7. This was obtained using ~3–4 nm as the radius of the NP and ~0.8 nm as the thickness of the outer shell, the latter being ~1 unit cell. This indicates that our Raman and XES spectra should be significantly affected by reaction with silicon at ambient conditions, which is not the case. Also, due to the sizable surface to core volume fraction, the XANES and XMCD spectra should be significantly affected if a major chemical reaction with the silicon oil takes place as the pressure is increased (this will be discussed later). Raman spectra of NPs were obtained in the presence and in the absence of silicon oil pressure medium at ambient conditions to probe for any changes induced by reaction with the pressure medium. The spectra were obtained with a low power laser (~6 mW) over a short time interval of a few minutes to avoid heat-induced phase changes in the NPs, explaining the relatively noisy data. The frequencies and relative intensities of peaks in the Raman spectra with and without silicon oil are very similar to one another. For comparison, formation of a magnetite-like structure would have produced a very pronounced A_{1g} mode roughly ten-fold stronger than the other peaks, which was not observed [18]. Similarly, formation of iron-oxide phases other than maghemite and magnetite would have resulted in significant changes in Raman intensity which was not observed [18]. Therefore, the addition of silicon oil pressure medium at ambient pressure does not cause a transition into a magnetite-like structure, which is only observed under pressure.

Our XES spectra taken in the presence/absence of silicon oil pressure medium with the difference spectrum is seen in figure 2(b). Except for a small dip in intensity of the main peak, significant changes in spectra were minimum. We observed an IAD value of 0.023 ± 0.002 when the silicon oil was added to NPs.

3.3. XANES spectra of NPs

XANES spectra of bulk magnetite and maghemite reference samples are similar to previously published results [15]. The low-energy, weak pre-edge peak is sensitive to the Fe 3*d*

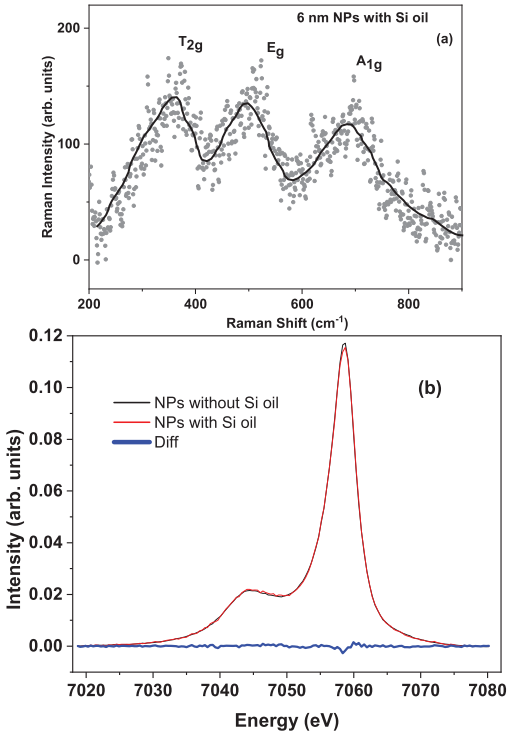

Figure 2. Raman spectra of NPs (a) in the presence of pressure medium, silicone oil with phonon peak assignments. (b) XES spectra of NPs normalized to area in the presence and absence of pressure medium Si oil, with the difference spectra (Diff).

character of empty Fe 3*d*-4*p* hybridized states at the Fermi level whereas the intense main-edge peak at higher energy is mainly sensitive to the Fe 4*p* character [33].

The pre-edge intensity, shape and energy are usually sensitive to spin states, deviation from centrosymmetry, ligand field strength and 3*d*-4*p* mixing, whereas the main-edge and higher energy region is used to estimate coordination number and oxidation state. Previous studies discuss that the XANES pre-edge signal in bulk maghemite and magnetite primarily originates from Fe^{3+} at tetrahedral sites and the lack of inversion symmetry at tetrahedral sites leads to 3*d*-4*p* mixing. [34, 35].

XANES data at ambient conditions (without silicon oil) show that the chemical and electronic structure of NPs is more similar to bulk maghemite than to bulk magnetite, in agreement with previous studies [15] and with the Raman data. As it is inadequate to consider that stoichiometric bulk standards coexist in the confined space of NPs [15], any quantitative XANES linear combination analysis of NPs with bulk reference standards has not been attempted. Due to disorder caused by size constraint, vacancies that appear in nominal magnetite NPs give rise to a structurally adapted intermediate state between bulk magnetite and bulk maghemite. Nano counterparts of magnetite and maghemite are reported to have cell parameters less than ~8.39 Å [36] and ~8.36 Å [37] respectively, agreeing with those of NPs in this study.

3.3.1. XANES pre-edge and main edge at high pressure. The intensity and peak energy of the pre-edge region of NPs show interesting behavior with increasing and decreasing pressure (figure 3). The integrated area of the pre-edge feature (from ~7.110 keV to ~7.116 keV) is shown in figure 3(a). It is used to quantify the variation of pre-edge intensity with pressure. As the pre-edge feature shows broadening as well as decrease in peak intensity with pressure, it is integrated over a sufficiently large energy range to capture the ensuing changes. As pressure is increased, there's no appreciable change in the peak area up to ~13 GPa. From ~13 GPa to ~19 GPa, a sharp gradual decrease in pre-edge intensity by ~30% is seen. These features can be attributed to either an increase in coordination number, change in coordination symmetry, or a change in oxidation state of Fe. The NP pre-edge feature is compared to those of the bulk standards, magnetite and maghemite (see the inset of figure 3(d)). As the pressure is increased, the similarities of the pre-edge of NPs compared to those of bulk maghemite, in terms of intensity and shape, disappear indicating a change in bonding environment of Fe. There is a shift in the energy position of this peak toward low energies starting around ~10 GPa indicating a reduction of Fe oxidation state (increase in occupied 3*d* states).

The main, leading edge of XANES spectra originates from electron transitions into empty states with Fe 4*p* character. The main-edge shows a shift in edge energy to lower energies with pressure (figures 3(b)–(d)). This shift is significant after ~10 GPa (figure 3(b)). This indicates a reduction in the oxidation state of Fe and agrees with the shift in pre-edge peak as discussed before. It's also important to note that, the spectral weight of main-edge features increases with pressure. It is significant after ~10 GPa as there's a sharp increase in the main-edge intensity (figures 3(c) and (d)). This indicates an increase in empty Fe 4*p* character.

Further, the main-edge region is compared to those of bulk standards, magnetite and maghemite in figures 3(c) and (d). Bulk maghemite shows significant resolvable features on the rising main edge, around ~7124 eV and ~7128 eV. These features are transitions to empty orbitals with Fe 4*p* character. As the pressure is increased, the features at ~7124 eV and ~7128 eV in the NPs smear out appreciably. In fact, our lowest pressure ~0.5 GPa already shows appreciable disappearance of these features. At the highest pressure (19.8 GPa), the main edge is shifted to energies lower than both bulk standards (figures 3(c) and (d)), indicating the existence of a lower oxidation state of Fe in NPs compared to those of the bulk standards.

Both the pre-edge and the main-edge of NPs around ~12 GPa are compared to those of bulk magnetite in figure 4. XANES spectrum appears to replicate features of bulk magnetite around ~12 GPa. However, the pre-edge feature remains suppressed and does not match that of bulk magnetite.

Figure 3 shows the evolution of NP XANES data during the decompression process as well. The NP XANES regions (pre-edge or main-edge) do not recover their original spectra in contrast to bulk magnetite investigations [7, 38]. The pre-edge intensity and the main-edge shift remains fairly constant during decompression (figures 3(a) and (b)). The pre-edge intensity remains suppressed indicating that any changes associated with coordination number, coordination symmetry and/or oxidation state in the tetrahedral sites of Fe at high pressure are irreversible (see the inset of figure 3(f)). The irreversibility of main-edge shift also supports the irreversibility of the

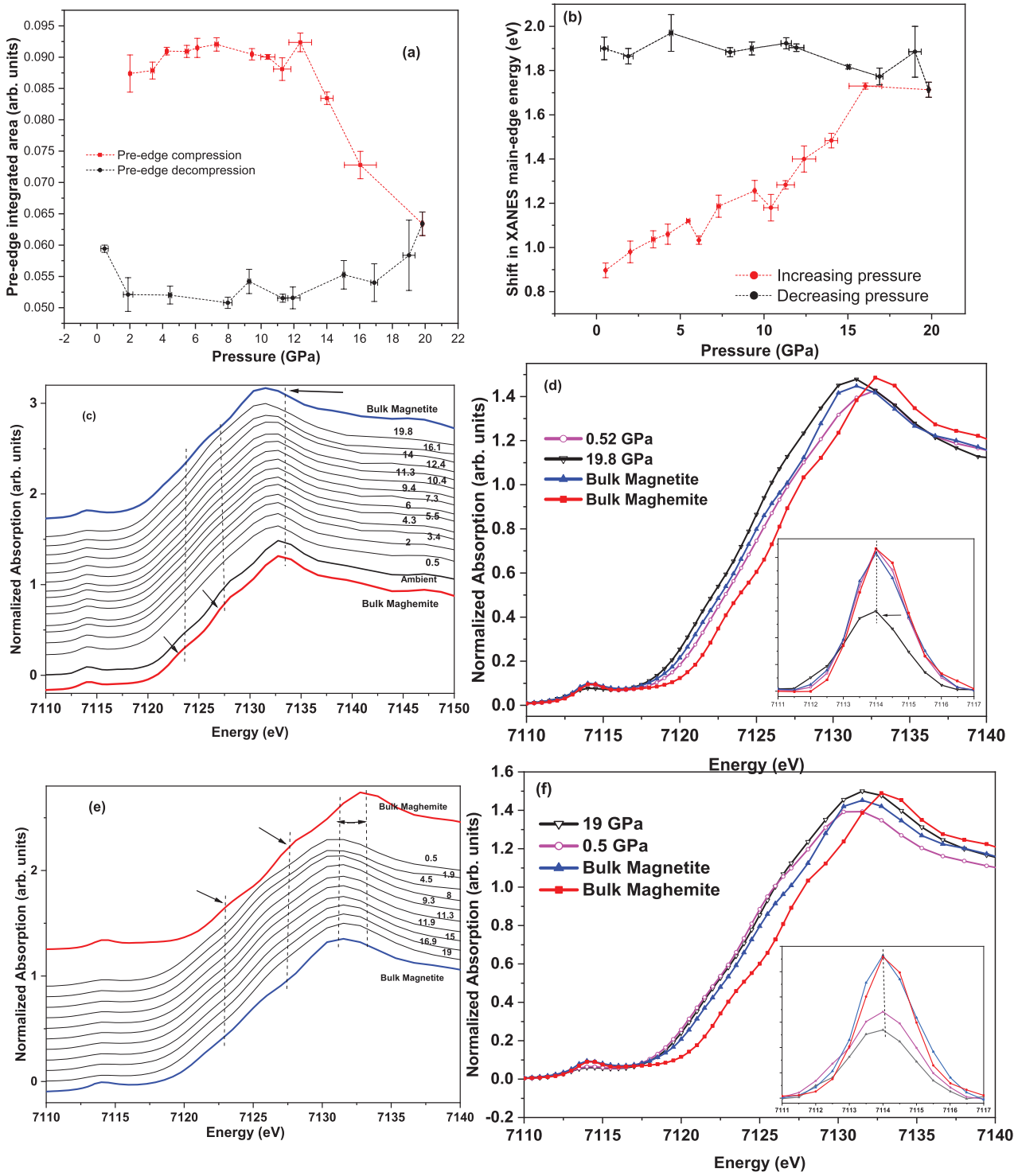

Figure 3. (a) The integrated area of the absolute value of the XANES pre-edge integral (the error bars represent the standard deviation of data at each pressure value, the pressure values are in GPa) (b) main edge-shift in NP XANES with respect to that of bulk maghemite (c) XANES of NPs compared with bulk standards, at high pressure (d) XANES corresponding to lowest and highest-pressure values at high pressure for clarity (e) XANES of NPs compared with bulk standards, at decompression (f) XANES corresponding to lowest and highest-pressure values at decompression for clarity.

oxidation state of Fe in NPs. Similarly, as seen in figures 3(e) and (f), the NP XANES spectra do not recover their structural features in the main-edge (features in bulk maghemite around ~7124 eV and ~7128 eV, seen in the NP sample at ambient conditions). The main-edge fine structure of decompressed NPs does not show any similarities to that of bulk maghemite after decompression. We cannot explain the exact reason for this irreversibility, but we assume that defects present in the initial NP structure undergo a transformation under pressure.

In Baudelet *et al* [7], a shift of the extended x-ray-absorption fine structure (EXAFS) oscillation to higher energies is seen under pressure due to the compression of interatomic

distances. While a slight increase in the intensity of the white line is observed, the line shape does not change indicating structural stability. In Ding *et al* [6], the XANES spectra do not change with pressure indicating the absence of structural changes. In contrast, the line shape of NP XANES in the current study changes even at ~0.5 GPa indicating a structural change from maghemite-like to magnetite-like starting at low pressure. These contrasting features of bulk materials versus NPs at high pressure can be attributed to nanoscale effects.

3.4. X-ray magnetic circular dichroism (XMCD)

We used Fe *K*-edge XMCD as an indirect measure of the 3*d* magnetic moment as described previously. This technique can identify contributions from Fe(III) and Fe(II) ions in tetrahedral versus octahedral sites [39].

Figures 5(a)–(c) show the evolution of Fe *K*-edge XMCD spectra of NPs with pressure. Figures 5(a) and (b) display two dispersion type XMCD signals at the pre-edge and at the main-edge region with opposite signs. Previous studies show that both bulk magnetite and maghemite display similar (in energy position and shape) XMCD signals at the pre-edge and at the main-edge. [34, 38, 39] In the pre-edge region however, bulk magnetite XMCD displays a negative small peak around 7112.9 eV [34]. The signal to noise ratio in our XMCD signals makes it difficult to determine any existence of this type of feature in our NPs.

Previous studies discuss that the pre-edge XMCD signal in bulk maghemite and magnetite originates from Fe^{3+} located at tetrahedral sites [34, 35]. As discussed below, this assumption appears to be validated by FEFF8 simulations of the Fe *K*-edge XMCD spectra. This leads us to assume that the pre-edge XMCD signal in our NPs originates from Fe^{3+} located at tetrahedral sites at both ambient and at high pressure. In the main-edge region, there is a negative to positive dispersion type XMCD signal. Previous studies on bulk standards indicate that there is no clear knowledge to whether the origin of this signal is attributed to Fe ions in either octahedral or tetrahedral or from both sites [6, 7, 40, 41]. Our FEFF8 theoretical calculations on bulk magnetite show that the low energy part of this signal has contributions from both octahedral and tetrahedral sites while the high energy part is dominated by octahedral sites (figure 6). Therefore, the main-edge XMCD can be used as a measure of the total magnetization in bulk magnetite structure. As our NPs possess similar main-edge features to bulk magnetite at various pressure values, we consider that the main-edge XMCD in NPs originates from both tetrahedral and octahedral sites. Therefore, insights into the evolution of net magnetization of NPs at various pressure values could be obtained from the main-edge XMCD signal as indicated by Baudelet *et al* [7].

The integrated absolute area of the pre-edge XMCD feature of NPs (from 7.110 keV to 7.116 keV) is shown in figure 5(c), which quantifies the variation of amplitude of XMCD spectra with pressure. The integral remains close to zero as seen in previous bulk magnetite investigations [6, 7] indicating a near quenching of 4*p* orbital moment. This integral shows a

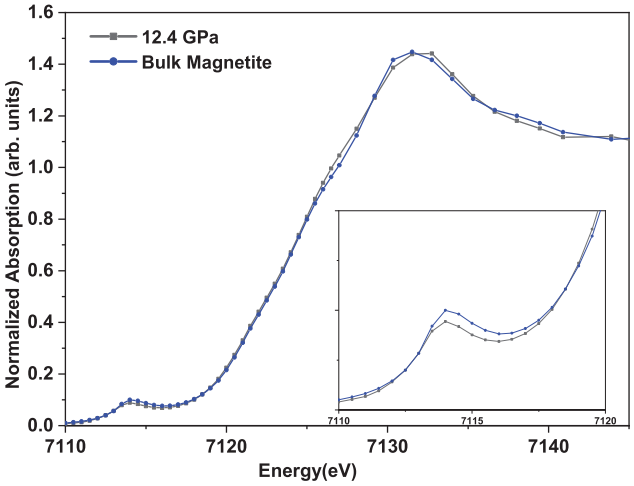

Figure 4. NP XANES that produce similar features to those of bulk standard, magnetite, at ~12 GPa.

weak decrease of ~14% up to ~10 GPa and a sharp decrease of ~42% thereafter. Overall, it indicates a reduction in magnetic moment totaling ~50% at the highest pressure. The integrated absolute area of the main-edge XMCD signal shows a similar behavior to that of the pre-edge XMCD signal (figure 5(c)). Up to ~15 GPa, a weak decrease of ~15% is followed by a sharp decrease of ~36%. The overall decrease in the net magnetic moment totals to ~46% at the highest-pressure value.

In terms of bulk magnetite, either a continuous or an abrupt decrease in the magnetic moment based on XMCD signal has been reported. As an example, Subias *et al* [38] show a continuous variation of this integral where it remains fairly constant up to ~15 GPa and drops by ~50% around 25 GPa. Similar results have been reported by Baudelet *et al* [7]. However, Ding *et al* [6] shows an abrupt (~50%) reduction of the XMCD signal between ~12 and ~16 GPa.

In bulk magnetite, the opposite signs of the two XMCD peaks (pre-edge A-A′ and main-edge B-B′) indicate the existence of ferrimagnetic order between tetrahedral and octahedral sites [7] with a saturation magnetization of 4 μ_B per formula unit. Although the NP XMCD signal shows similar features to those of bulk magnetite, the saturation magnetization calculated from the hysteresis loop of NPs (figure 1(e)) at room temperature is ~2.3 μ_B per formula unit. The reduction in magnetization in the NPs at ambient conditions is expected as a result of surface spin disorder and possible influence of structural defects. It is important to note that, within our pressure range, the net magnetization remains non-zero as seen by the non-vanishing XMCD signal, albeit with a suppression of net magnetization under pressure.

3.5. X-ray emission spectroscopy (XES)

To probe whether the reduction of XMCD intensity at high pressures is related to a reduction of local moment (as opposed to ordered moment) we use high resolution non-resonant XES. It leverages the exchange interaction between the 3*p* core hole and the 3*d* magnetic moment and is very sensitive to the local magnetic moment although it is insensitive to the magnetic

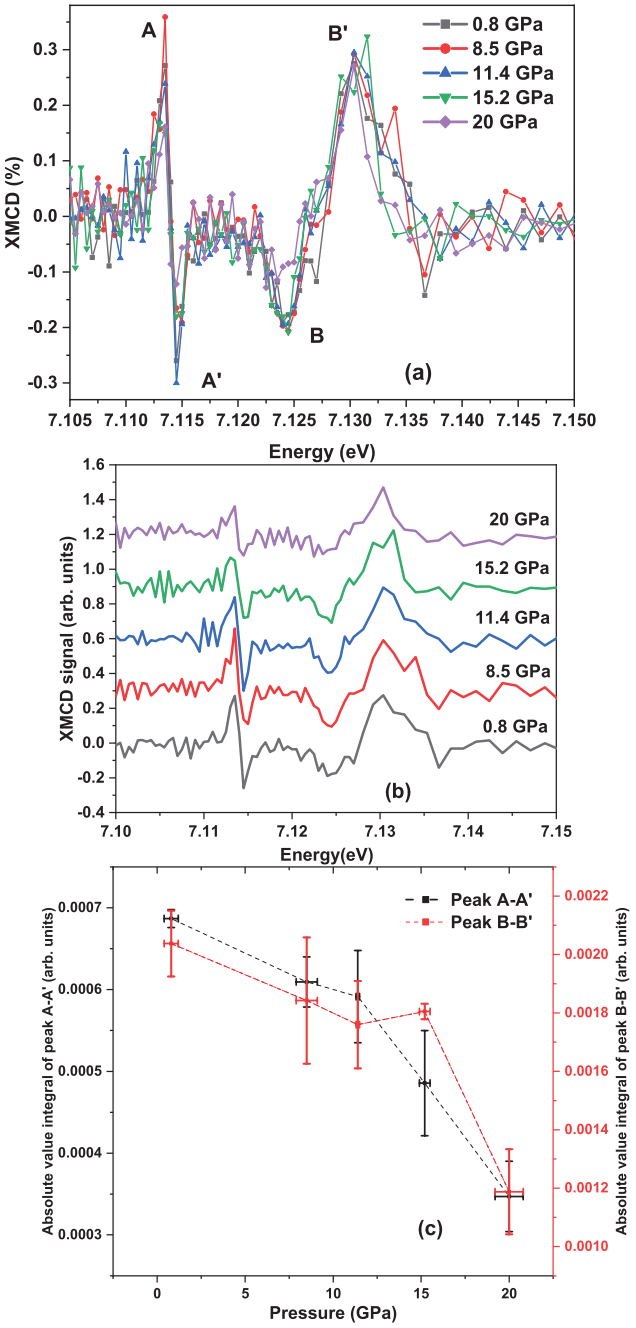

Figure 5. (a) XMCD of NPs at high pressure (b) XMCD of NPs plotted separately for clarity (c) the absolute value integrals of peaks AA′ and BB′ at compression (the error bars represent the standard deviation of data at each pressure value).

ordering of the sample [42]. In Fe, the emission spectrum of high spin (HS) state is characterized by a main peak, $K_{\beta_{1,3}}$ with an energy of 7058 eV and a satellite peak, $K_{\beta'}$ located ~12 eV towards the lower energies. A disappearance of the satellite peak indicates the transition of Fe to a low spin (LS) state through the collapse of the 3*d* magnetic moment. Also, a shift in the main XES peak towards the low energies indicates a variation from a HS to a LS state [43].

As seen in figures 7(a)–(c), in the presence of silicon pressure medium, as the pressure is increased, the main peak exhibits a shift towards low energies indicating a change in

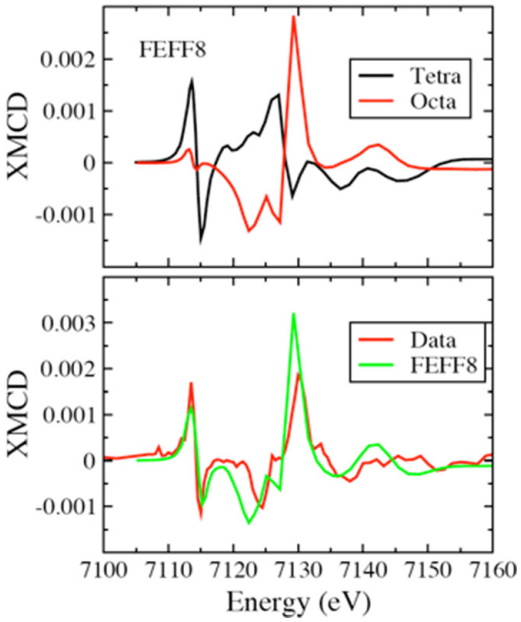

Figure 6. Calculated XMCD pre-edge and main-edge components of bulk magnetite based on contributions from tetrahedral and octahedral sites (using FEFF8 code).

the total spin. The intensity of the satellite peak is proportional to the number of unpaired 3*d* electrons. We observe a clear reduction in the intensity of this peak as the pressure is increased. Both features agree with a variation from a HS state. By subtracting the spectrum at the ambient pressure (~1 bar) from each spectrum at each pressure value and obtaining the integral of the absolute value of the difference spectra (IAD) [30, 44, 45], IAD analysis method provides only the relative values of spin states [45]. Therefore, our discussion on XES is restricted to the pressure-induced change in the spin state (i.e. HS, LS etc). We observe a continuous increase in the XES-IAD value up to ~27 GPa, with a more pronounced rate of increase above ~6–7 GPa. These changes indicate a continuous reduction of the local spin moment (figure 7(c)). The changes in XES-IAD appear to be reversible upon decompression, although the scatter in the data prevents us from ruling out some irreversibility upon return to ambient pressure.

In bulk magnetite investigations [6] a reduction in the XES intensity around ~15 GPa has been observed and it was attributed to a transition between HS and intermediate spin (IS) states. This observation was associated with an abrupt, discontinuous reduction in the XMCD signal between 12 and 16 GPa. Our data is inconsistent with a sharp spin transition but consistent with a gradual, continuous pressure-induced change in spin configuration away from a high-spin state.

It is important to note that we investigated whether there were any interactions between the NPs and silicon oil at ambient conditions using XES (figure 2(b)). As discussed before, a very small change in the main XES peak was observed when adding silicon oil, with the IAD value being comparable to IAD values obtained up to ~6 GPa. Significant changes in XES spectra are only observed above 6–7 GPa, where the shift in main peak towards low energies and a decrease in satellite intensity starts appearing in spectra. Therefore, we conclude

that although we cannot rule out an interaction between the oil and the NP surface at ambient conditions, it appears that this interaction does not dominate the evolution of the data under pressure.

4. Discussion

4.1. Possible explanations for the evolution of electronic and magnetic properties of NPs.

High pressure could initiate a reaction between the NPs and the pressure medium. It's important to discuss whether there could be any interaction of NPs with silicone oil at high pressure. As discussed before, if NPs interacted with silicone oil at ambient and high-pressure conditions, 70% of the volume of the NP would be affected, and spectroscopic features in XANES and XMCD spectra are expected to be significantly affected. We compared the evolution of spectral features in XANES spectra under pressure to see if such evolution could indicate formation of Fe_2SiO_4 [46], FeH [47], goethite (FeO(OH)) [48], hematite(alpha-Fe_2O_3) [49] and wurtzite (FeO) [49] as a result of reaction with silicon oil. We see no evidence for a sizable contribution from any of these compounds to the XANES spectra. At ambient conditions, although the XES spectra show an increase in IAD value after the addition of silicone oil, the nature of this change is significantly different from what is observed at high pressure where significant features such as a shift in the main peak towards lower energies and a decrease in satellite peak intensity are observed. Hence, although we cannot rule out an interaction between the oil and the NP surface, based on our comparisons, it appears that this interaction does not dominate the evolution of the data under pressure. This is because, if there is an interaction, ~70% of the atoms on the NPs would be affected and significant changes in spectroscopic features would take place (certainly for the XMCD line shape which relies on the antiferromagnetic coupling of Fe at octahedral and tetrahedral sites as seen in figure 6). The compact nature of the NPs, unlike nanotubes or clatharate cages as described in San-Miguel [3], is not conducive to intercalation and any interaction with the pressure medium would be surface-driven. Also, the change of NP XANES from maghemite-like to magnetite-like under pressure provides strong evidence for a pressure-driven change in local structure from maghemite-like to magnetite-like phase, not a significant chemical interaction with the silicon oil.

An important observation in our study is that the NPs start deviating from bulk maghemite-like phase (all sites occupied by Fe^{3+}) right at the initial pressure increase and assume bulk magnetite-like phase (combination of Fe^{2+} and Fe^{3+}) around ~12 GPa as seen in the XANES spectra. Note that both bulk magnetite and maghemite possess cubic inverse spinel structures. The reduction of the Fe oxidation state is clearly seen in the shift associated with the pre-edge and the main-edge energies to lower energies. However, this reduction extends to more lower energies as the pressure is increased, indicating converting the remaining Fe^{3+} to Fe^{2+} in the bulk magnetite-like structure. Therefore, interpretations of the results on NPs need knowledge of the response of both bulk magnetite and maghemite to high pressures.

High pressure XRD studies on bulk magnetite have seen no structural transitions in the pressure range, 4 GPa to 18 GPa [6] although previous research suggested a reversible phase transition in the same pressure range [50]. In maghemite, both bulk and nanocrystalline phases (5 nm) undergo a structural phase transition to hematite (α-Fe_2O_3) at 16 GPa [51]. Although bulk hematite is an antiferromagnet, its nanocounterpart may not have the same magnetic properties as the bulk due to spin disorder [52–56]. Therefore in the case of a phase transition to hematite-like structure, the net XMCD signal could be reduced. However, the XANES spectra of our NPs at different pressures do not show features similar to those of bulk hematite (as discussed before) indicating the absence of a similar structural transition that would affect the total magnetic moment of the NPs.

A possible basic explanation for the decrease in magnetic moment in the NPs is charge transfer from Fe 4*p* to 3*d* states reducing the number of unpaired 3*d* electrons (oxygen 2*p* orbitals, which hybridize with Fe 3*d* orbitals, may also participate in this charge transfer).

Note that from initial pressure increase, the oxidation state of Fe decreases (disappearance of high-spin Fe^{3+} with $3d^5$ electrons and appearance of more Fe^{2+} with $3d^6$ electrons). The continuous decrease of our XES signal is consistent with a reduction in the number of Fe ions in the high-spin state. Note that our data does not show any sudden discontinuities in spin state as previously reported in XMCD studies of bulk magnetite [6].

The behavior of our XMCD signal at high pressure is more in line with work done by Baudelet *et al* [7] and Subias *et al* [38]. Hence, in our sample the decrease in XMCD intensity could be explained by a gradual charge transfer from Fe 4*p* to 3*d* states that results in a gradual change in Fe spin state. It is important to note that the evolution of pre-edge and main-edge XANES spectra with pressure are quite different than reported for bulk magnetite at high pressure [6, 7, 38].

In bulk magnetite, the reduction in net magnetic moment is explained in terms of a band structure description [7], namely, broadening of the majority spin valence band until it crosses the Fermi level which results in a reduction of the magnetic moment. This observation is not followed by a structural transition [7]. Friak *et al* [57] also mentions that due to the broadening of the majority spin band, the material undergoes a half metal to metal transformation. This leads to the majority spin-valence band states near the Fermi level getting depopulated in favor of minority spin-valence band reducing the magnetic moment by about 1%. However, this decrease in the magnetic moment is very small compared to what we observe in NPs (~50%). It's rare to find calculations that study whether spin transitions similar to bulk magnetite would occur in bulk maghemite at high pressure or not.

Therefore, the aforementioned band structure description could be another valid explanation for the behavior of NPs. However, note that the changes associated with the NP XANES pre-edge shape, intensity and energy position clearly suggest changes in local environment around Fe at tetrahedral

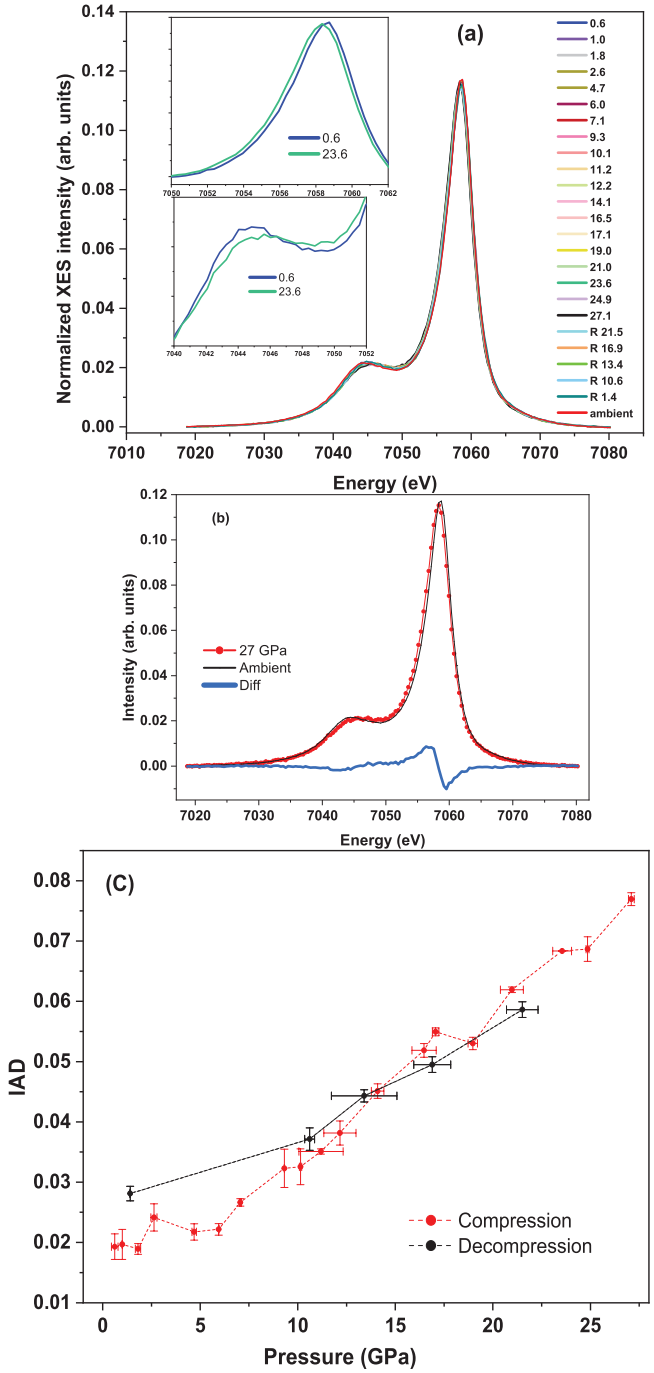

Figure 7. (a) Normalized XES intensity (normalized by the area) of NPs with silicon oil as the pressure medium. (Pressure values are in GPa. '*R*' stands for pressure release. 'Ambient' stands for the NPs sample without silicon oil at ambient (~1 bar) conditions.) (b) An example XES spectra (27 GPa) is shown in red while the reference spectrum (sample at ambient conditions) is shown in black. The difference spectrum (Diff) is shown in blue (c) IAD as a function of pressure obtained by subtracting the reference from each scan and obtaining the integral of the absolute value of the difference spectrum upon compression (red) and decompression (black). Error bars represent the standard deviation of data at each pressure value.

sites. Therefore, our NPs undergo a reduction in the net magnetic moment in the presence of a reduction in Fe oxidation state and a change in the local environment around Fe at tetrahedral sites. Upon decompression, the XANES spectra of NPs do not recover their original structure. This indicates that NPs behave differently in terms of reversibility of structural changes to those of bulk.

Based on a sharp decrease in pre-edge intensity, a change in slope in the rate of main -edge shift with pressure, and a change in slope in XMCD integrals at ~12 GPa, and noting that the NP XANES spectra assume the shape of bulk magnetite at ~12 GPa, we conclude that this pressure is a crossover pressure where the maghemite-like NPs are mostly converted into magnetite-like structure.

5. Conclusions

In this study, we investigate the evolution of electronic and magnetic properties of nominal magnetite NPs at high pressure in the presence of silicone oil as the pressure medium.

The absolute integral of the XANES pre-edge region shows a decrease starting at ~14 GPa continuing up to the highest pressure of 20 GPa (30% total reduction). This indicates a reduction of empty 3*d* orbitals, a change in the oxidation state of Fe and the local environment around Fe at tetrahedral sites. Both pre-edge and the main-edge shift to lower energies starting around ~10 GPa supporting a reduction in the Fe oxidation state. This is accompanied by an increase in the main-edge spectral weight due to an increase in the empty density of states with Fe 4*p* orbital character (i.e. reduction of occupied Fe 4*p* states). By looking at the whole XANES spectra, the NPs deviate from those of bulk maghemite (all sites occupied by Fe^{3+}) starting with the first pressure increase at ~0.5 GPa. The NPs assume a bulk magnetite-like phase at about 12 GPa (combination of Fe^{2+} and Fe^{3+}). Even after ~12 GPa, the spectra continue to shift to lower energies, indicating conversion of the remaining Fe^{3+} to Fe^{2+} in the magnetite-like structure. These changes are not recoverable at decompression. These features of XANES spectra are very different from those of bulk magnetite investigations which show no significant pre-edge or main-edge changes under pressure.

Regarding the XMCD spectra, an overall total magnetic moment suppression of ~50% is seen at the highest pressure, although the net magnetization remains finite. The reduction in XMCD signal is continuous. Similar suppression is seen in XMCD studies of bulk magnetite. XES spectra of NPs indicate a gradual reduction in Fe spin moment, consistent with the continuous charge transfer from Fe 4*p* to 3*d* states seen in the XANES data and the reduction in XMCD signal. The reduction in Fe spin moment could be interpreted as due to a gradual charge transfer from *p* to *d* states leading to an IS state, or as due to a redistribution of electrons between exchange-split 3*d* bands induced by band broadening under pressure. It is important to note that in NPs, these changes in the net magnetic moment are associated with a reduction in oxidation state of Fe and modifications in local environment around Fe at tetrahedral sites, which are not observed in the case of bulk magnetite.

Therefore, in this study, we clearly observe new phenomena in the nano-counterparts of bulk magnetite at high pressure. These features could be attributed to nanoscale

effects originating from very small crystallite sizes, large surface-to-volume ratio, near-surface relaxation/ reconstruction, local lattice distortions, differences in types and densities of defect sites in NPs compared to their bulk-counterpart.

Acknowledgment

KW acknowledges the financial support received from the Department of Physics and Astronomy and from the Faculty Research Award provided by the Vice President of Research at the Graduate School, University of Maine, Orono, USA. We thank Dr Changyong Park at sector 16, Advanced Photon Source (APS), Argonne National Laboratory for an earlier attempt at this experiment with XANES. We thank Dr Robert Meulenberg for providing material and laboratory facilities for the preparation of NPs, Mr Stuart Lawson for NP preparation support, Dr Carl Tripp, Ms Sabrina Sultana for Raman spectroscopy support, Dr George Bernhardt for XRD support and Mr Alex Khammang for MPMS instrumentation support at the University of Maine, Orono. We thank Dr Adam Graham, Dr Jules Gardener and Dr James Reynolds at the Center for Nanoscience, Harvard University for conducting TEM imaging. We thank 4-ID-D (sector 4), Advanced Photon Source (APS), Argonne National Laboratory for providing beamtime for the experiment. Portions of this work were performed at HPCAT (Sector 16), Advanced Photon Source (APS), Argonne National Laboratory. HPCAT operations are supported by DOE-NNSA's Office of Experimental Sciences. The Advanced Photon Source is a U.S. Department of Energy (DOE) Office of Science User Facility operated for the DOE Office of Science by Argonne National Laboratory under Contract No. DE-AC02-06CH11357. Finally, we acknowledge the valuable comments given by the anonymous referees of the JPCM journal.

ORCID iDs

Kalpani Werellapatha https://orcid.org/0000-0002-9315-4054

References

[1] Nowack B and Bucheli T D 2007 Occurrence, behavior and effects of nanoparticles in the environment *Environ. Pollut.* **150** 5–22
[2] Banfield J F and Zhang H 2001 Nanoparticles in the environment *Rev. Miner. Geochem.* **44** 1–58
[3] San-Miguel A 2006 Nanomaterials under high-pressure *Chem. Soc. Rev.* **35** 876–89
[4] Waychunas G A, Kim C S and Banfield J F 2005 Nanoparticulate iron oxide minerals in soils and sediments: unique properties and contaminant scavenging mechanisms *J. Nanopart. Res.* **7** 409–33
[5] Moriarty P 2001 Nanostructured materials *Rep. Prog. Phys.* **64** 297
[6] Ding Y, Haskel D, Ovchinnikov S G, Tseng Y-C, Orlov Y S, Lang J C and Mao H 2008 Novel pressure-induced magnetic transition in magnetite (Fe_3O_4) *Phys. Rev. Lett.* **100** 045508
[7] Baudelet F, Pascarelli S, Mathon O, Itié J-P, Polian A and Chervin J-C 2010 Absence of abrupt pressure-induced magnetic transitions in magnetite *Phys. Rev.* B **82** 140412
[8] Mao H-K, Takahashi T, Bassett W A, Kinsland G L and Merrill L 1974 Isothermal compression of magnetite to 320 KB *J. Geophys. Res.* **79** 1165–70
[9] Huang E and Bassett W A 1986 Rapid determination of Fe_3O_4 phase diagram by synchrotron radiation *J. Geophys. Res. Solid Earth* **91** 4697–703
[10] Pasternak M P, Nasu S, Wada K and Endo S 1994 High-pressure phase of magnetite *Phys. Rev.* B **50** 6446–9
[11] Finger L W, Hazen R M and Hofmeister A M 1986 High-pressure crystal chemistry of spinel ($MgAl_2O_4$) and magnetite (Fe_3O_4): comparisons with silicate spinels *Phys. Chem. Miner.* **13** 215–20
[12] Noh J, Osman O I, Aziz S G, Winget P and Brédas J-L 2014 A density functional theory investigation of the electronic structure and spin moments of magnetite *Sci. Technol. Adv. Mater.* **15** 044202
[13] Jeng H-T and Guo G Y 2002 First-principles investigations of the electronic structure and magnetocrystalline anisotropy in strained magnetite Fe_3O_4 *Phys. Rev.* B **65** 094429
[14] Grau-Crespo R, Al-Baitai A Y, Saadoune I and De Leeuw N H 2010 Vacancy ordering and electronic structure of γ-Fe_2O_3 (maghemite): a theoretical investigation *J. Phys. Condens. Matter* **22** 255401
[15] Piquer C, Laguna-Marco M A, Roca A G, Boada R, Guglieri C and Chaboy J 2014 Fe K-edge x-ray absorption spectroscopy study of nanosized nominal magnetite *J. Phys. Chem.* C **118** 1332–46
[16] da Costa G M, de Grave E, de Bakker P M A and Vandenberghe R E 1995 Influence of nonstoichiometry and the presence of maghemite on the mossbauer spectrum of magnetite *Clays Clay Miner.* **43** 656–68
[17] Mørup S 1983 Mössbauer spectroscopy studies of suspensions of Fe_3O_4 microcrystals *J. Magn. Magn. Mater.* **39** 45–47
[18] Jubb A M and Allen H C 2010 Vibrational spectroscopic characterization of hematite, maghemite, and magnetite thin films produced by vapor deposition *ACS Appl. Mater. Interfaces* **2** 2804–2812
[19] De Faria D L A, Venâncio Silva S and De Oliveira M T 1997 Raman microspectroscopy of some iron oxides and oxyhydroxides *J. Raman Spectrosc.* **28** 873–8
[20] Oblonsky L J and Devine T M 1995 A surface enhanced Raman spectroscopic study of the passive films formed in borate buffer on iron, nickel, chromium and stainless steel *Corros. Sci.* **37** 17–41
[21] Feitknecht W and Gallagher K J 1970 Mechanisms for the oxidation of Fe_3O_4 *Nature* **228** 548
[22] Mathon O, Baudelet F, Itié J P, Polian A, d'Astuto M, Chervin J C and Pascarelli S 2004 Fe magnetic transition under high pressure *Phys. Rev. Lett.* **93** 255503
[23] Stähler S, Schütz G and Ebert H 1993 Magnetic *K*-edge absorption in 3*d* elements and its relation to local magnetic structure *Phys. Rev.* B **47** 818
[24] Schütz G, Wagner W, Wilhelm W, Kienle P, Zeller R, Frahm R and Materlik G 1987 Absorption of circularly polarized x rays in iron *Phys. Rev. Lett.* **58** 737
[25] Kim D K, Mikhaylova M, Zhang Y and Muhammed M 2003 Protective coating of superparamagnetic iron oxide nanoparticles *Chem. Mater.* **15** 1617–27
[26] Guardia P, Labarta A and Batlle X 2010 Tuning the size, the shape, and the magnetic properties of iron oxide nanoparticles *J. Phys. Chem.* C **115** 390–6
[27] Haskel D, Tseng Y C, Lang J C and Sinogeikin S 2007 Instrument for x-ray magnetic circular dichroism

measurements at high pressures *Rev. Sci. Instrum.* **78** 083904
[28] Ankudinov A L, Ravel B, Rehr J J and Conradson S D 1998 Real-space multiple-scattering calculation and interpretation of x-ray-absorption near-edge structure *Phys. Rev.* B **58** 7565
[29] Bunker G 2010 *Introduction to XAFS: a Practical Guide to X-ray Absorption Fine Structure Spectroscopy* (Cambridge: Cambridge University Press)
[30] Vankó G, Rueff J-P, Mattila A, Németh Z and Shukla A 2006 Temperature- and pressure-induced spin-state transitions in $LaCoO_3$ *Phys. Rev.* B **73** 02442
[31] Chernyshova I V, Hochella M F Jr and Madden A S 2007 Size-dependent structural transformations of hematite nanoparticles. 1. Phase transition *Phys. Chem. Chem. Phys.* **9** 1736–50
[32] Oh S J, Cook D C and Townsend H E 1998 Characterization of iron oxides commonly formed as corrosion products on steel *Hyperfine Interact.* **112** 59–66
[33] Yamamoto T 2008 Assignment of pre-edge peaks in K-edge x-ray absorption spectra of 3d transition metal compounds: electric dipole or quadrupole? *X-Ray Spectrom.* **37** 572–84
[34] Carvallo C, Sainctavit P, Arrio M-A, Menguy N, Wang Y, Ona-Nguema G and Brice-Profeta S 2008 Biogenic versus abiogenic magnetite nanoparticles: a XMCD study *Am. Miner.* **93** 880–5
[35] Sikora M, Juhin A, Weng T-C, Sainctavit P, Detlefs C, De Groot F and Glatzel P 2010 Strong *K*-edge magnetic circular dichroism observed in photon-in-photon-out spectroscopy *Phys. Rev. Lett.* **105** 037202
[36] Mürbe J, Rechtenbach A and Töpfer J 2008 Synthesis and physical characterization of magnetite nanoparticles for biomedical applications *Mater. Chem. Phys.* **110** 426–33
[37] Vidal-Vidal J, Rivas J and López-Quintela M A 2006 Synthesis of monodisperse maghemite nanoparticles by the microemulsion method *Colloids Surf.* A **288** 44–51
[38] Subías G, Cuartero V, García J, Blasco J, Lafuerza S, Pascarelli S, Mathon O, Strohm C, Nagai K and Mito M 2013 Investigation of pressure-induced magnetic transitions in $Co_xFe_{3-x}O_4$ spinels *Phys. Rev.* B **87** 094408
[39] Guyodo Y, Sainctavit P, Arrio M-A, Carvallo C, Lee Penn R, Erbs J J, Forsberg B S, Morin G, Maillot F and Lagroix F 2012 X-ray magnetic circular dichroïsm provides strong evidence for tetrahedral iron in ferrihydrite *Geochem. Geophys. Geosystems* **13**
[40] Maruyama H, Harada I, Kobayashi K and Yamazaki H 1995 Magnetic circular x-ray dichroism at Fe *K*-edge in ferrimagnetic Fe-oxides *Physica* B **208** 760–2
[41] Matsumoto K, Saito F, Toyoda T, Ohkubo K, Yamawaki K, Mori T, Hirano K, Tanaka M and Sasaki S 2000 Site-specific studies on x-ray magnetic circular dichroism at Fe *K* edge for transition-metal ferrites *Japan. J. Appl. Phys.* **39** 6089
[42] Badro J, Struzhkin V V, Shu J, Hemley R J, Mao H, Kao C, Rueff J-P and Shen G 1999 Magnetism in FeO at megabar pressures from x-ray emission spectroscopy *Phys. Rev. Lett.* **83** 4101–4
[43] Tsujimoto Y, Nakano S, Ishimatsu N, Mizumaki M, Kawamura N, Kawakami T, Matsushita Y and Yamaura K 2016 Pressure-driven spin crossover involving polyhedral transformation in layered perovskite cobalt oxyfluoride *Sci. Rep.* **6** 36253
[44] Rueff J-P, Kao C-C, Struzhkin V V, Badro J, Shu J, Hemley R J and Mao H K 1999 Pressure-induced high-spin to low-spin transition in FeS evidenced by x-ray emission spectroscopy *Phys. Rev. Lett.* **82** 3284–7
[45] Lengsdorf R, Rueff J-P, Vankó G, Lorenz T, Tjeng L H and Abd-Elmeguid M M 2007 Spin-state-driven metal-insulator transition in (La, Sr)CoO_3 *Phys. Rev.* B **75** 180401
[46] Abe Y, Iizawa Y, Terada Y, Adachi K, Igarashi Y and Nakai I 2014 Detection of uranium and chemical state analysis of individual radioactive microparticles emitted from the fukushima nuclear accident using multiple synchrotron radiation x-ray analyses *Anal. Chem.* **86** 8521–5
[47] Bouldi N, Sainctavit P, Juhin A, Nataf L and Baudelet F 2018 Electronic and magnetic properties of iron hydride under pressure: an experimental and computational study using x-ray absorption spectroscopy and x-ray magnetic circular dichroism at the Fe *K* edge *Phys. Rev.* B **98** 064430
[48] Sánchez-Marcos J, Laguna-Marco M Á, Martínez-Morillas R, Céspedes E, Jiménez-Villacorta F, Menéndez N and Prieto C 2011 Exchange bias in iron oxide nanoclusters *J. Phys.: Condens. Matter* **23** 476003
[49] Lv D, Wen W, Huang X, Bai J, Mi J, Wu S and Yang Y 2011 A novel Li_2FeSiO_4/C composite: synthesis, characterization and high storage capacity *J. Mater. Chem.* **21** 9506–12
[50] Rozenberg G K, Amiel Y, Xu W M, Pasternak M P, Jeanloz R, Hanfland M and Taylor R D 2007 Structural characterization of temperature-and pressure-induced inverse ↔ normal spinel transformation in magnetite *Phys. Rev.* B **75** 020102
[51] Zhu H, Ma Y, Yang H, Ji C, Hou D and Guo L 2010 Pressure induced phase transition of nanocrystalline and bulk maghemite (γ-Fe_2O_3) to hematite (α-Fe_2O_3) *J. Phys. Chem. Solids* **71** 1183–6
[52] Bødker F, Hansen M F, Koch C B, Lefmann K and Mørup S 2000 Magnetic properties of hematite nanoparticles *Phys. Rev.* B **61** 6826–38
[53] Mørup S, Brok E and Frandsen C 2013 Spin structures in magnetic nanoparticles *J. Nanomater.* **2013** 720629
[54] Mørup S, Madsen D E, Frandsen C, Bahl C R H and Hansen M F 2007 Experimental and theoretical studies of nanoparticles of antiferromagnetic materials *J. Phys.: Condens. Matter* **19** 213202
[55] Bødker F and Mørup S 2000 Size dependence of the properties of hematite nanoparticles *Europhys. Lett.* **52** 217
[56] Tadic M, Panjan M, Damnjanovic V and Milosevic I 2014 Magnetic properties of hematite (α-Fe_2O_3) nanoparticles prepared by hydrothermal synthesis method *Appl. Surf. Sci.* **320** 183–7
[57] Friák M, Schindlmayr A and Scheffler M 2007 Ab initio study of the half-metal to metal transition in strained magnetite *New J. Phys.* **9** 5